Heliyon 5 (2019) e02428

Contents lists available at ScienceDirect

Heliyon

journal homepage: www.heliyon.com

Effect of Mo on the catalytic activity of Ni-based self-organizing catalysts for processing of dichloroethane into segmented carbon nanomaterials

Yury I. Bauman [a], Yulia V. Rudneva [b], Ilya V. Mishakov [a,c], Pavel E. Plyusnin [b,c], Yury V. Shubin [b,c], Denis V. Korneev [d], Vladimir O. Stoyanovskii [a], Aleksey A. Vedyagin [a,e,*], Roman A. Buyanov [a]

[a] Boreskov Institute of Catalysis, pr. Lavrentieva 5, Novosibirsk, 630090, Russia
[b] Nikolaev Institute of Inorganic Chemistry, pr. Lavrentieva, Novosibirsk, 630090, Russia
[c] Novosibirsk State University, Pirogova Str. 2, Novosibirsk, 630090, Russia
[d] Monash University, Melbourne, 3800, Australia
[e] National Research Tomsk Polytechnic University, pr. Lenina 30, Tomsk 634050, Russia

ARTICLE INFO

Keywords:
Materials science
Carbon nanofibers
Bulk Ni-Mo alloy
Self-organizing catalysts
Segmented structure
Self-disintegration
Kinetics of carbon deposition
Catalysis
Heterogeneous catalysis
Heterogeneous methods

ABSTRACT

A series of micro-disperse Ni-Mo alloys with the sponge-like structure was prepared by a simultaneous precipitation method followed by sintering of the sediment in H_2 atmosphere at 800 °C. According to XRD data, the formation of single-phase solid solution $Ni_{1-x}Mo_x$ took place for the samples with Mo content of 0.6–8.3 wt.%. Synthesized samples were studied in a process of the catalytic CVD of $C_2H_4Cl_2$ at 550–700 °C. In situ kinetic studies of carbon deposition process were carried out in a flow gravimetric setup equipped with McBain balances. An interaction of Ni-Mo alloys with $C_2H_4Cl_2$ is accompanied by their rapid disintegration with formation of disperse active particles catalyzing the growth of carbon nanomaterials (CNM). The strong boosting effect of Mo on the catalytic performance of Ni was revealed. The maximum yield of CNM product (8.3 wt.% Mo, 600 °C, 120 min) was as high as 45 g/g_M. The study on effect of the reaction temperature on the CNM yield allowed one to define an optimal temperature regime. The impact of Mo concentration upon the morphology, structural features and textural properties of the produced carbon fibers was investigated by means of SEM, TEM, Raman spectroscopy and low-temperature nitrogen adsorption. The role of chemisorbed chlorine species in a pulse-to-pulse regime of the segmented carbon filaments formation was discussed.

1. Introduction

Carbon nanofibers (CNF) are one of the most important sorts of carbon nanomaterials (CNM), which is being extensively studied in recent years. Due to their advanced physicochemical and mechanical properties, carbon nanofibers attract much attention for application in various fields of nanotechnology, ranging from high-strength composites to energy storage materials [1, 2]. Catalytic chemical vapor deposition (CCVD) is the most widely used method for CNM synthesis, since it is capable of providing high yield of carbon product, good selectivity and opportunity for scale-up production [1, 2, 3, 4]. Implementation of the catalytic CVD allows one to tune the process parameters for production of vapor-grown carbon nanofibers of various structural types and different degree of graphitization [4].

Hydrocarbons (HC) are known as common precursors for CCVD synthesis of CNM. Meanwhile, usage of functionalized HC (substituted with Cl, N etc.) permits one to expand the assortment of nanostructured carbon materials [5, 6, 7]. For instance, the chlorinated HC can be used as a carbon source in catalytic CVD process similarly to unsubstituted ones [7, 8, 9, 10]. The decomposition of halogenated HC usually requires an addition of hydrogen excess to the reaction mixture, particularly in the case of polychlorinated HC ($CHCl_3$, C_2HCl_3 etc.). It is also worth noting that the catalytic CVD of chlorinated HC into CNM is now considered as one of the most effective ways for utilization of the hazardous organochlorine wastes [11, 12, 13, 14].

Nickel-based catalysts are commonly used for decomposition of chlorinated HC as Ni is the most resistant to deactivation by chlorine among the iron subgroup metals (Fe, Co, Ni) known to be active in CCVD process [9]. Nevertheless, the supported Ni-catalysts synthesized through the conventional coprecipitation or impregnation techniques are turned to be inclined

* Corresponding author.
E-mail address: vedyagin@catalysis.ru (A.A. Vedyagin).

https://doi.org/10.1016/j.heliyon.2019.e02428
Received 18 February 2019; Received in revised form 23 May 2019; Accepted 3 September 2019

to a rapid deactivation which might be caused by the chlorination or encapsulation of active particles with amorphous carbon [10]. With the purpose to avoid this disadvantage, a novel approach to prepare so-called "self-organizing" catalysts for the CNM synthesis was recently proposed [10, 11, 12, 13, 14, 15]. The developed method is based on using the bulk Ni-based alloys as a catalyst precursor to be subjected to controllable process of a metal dusting (MD) [15]. This process implies spontaneous disintegration of the bulk metallic alloys, which is forced by the corrosive action of the carburizing atmosphere in a temperature range of 400–800 °C [16]. MD (or carbon erosion) process ultimately results in emergence of the submicron metallic particles functioning as active centers for the catalytic growth of filamentous carbon. The self-organizing catalysts were shown to possess very good resistance to deactivation in course of CCVD of 1, 2-dichloroethane (DCE) providing an extremely high yield of CNM in the longevity tests (>400 g/g_{Ni}) [12].

The decomposition of $C_2H_4Cl_2$ over Ni-containing catalysts is known to occur via two reaction paths depending on the temperature and hydrogen concentration in the reaction mixture [13]. At elevated temperatures (500 °C and above) and moderate excess of H_2 in reaction gas, the carbide cycle mechanism prevails driving the process in accordance with the following reaction scheme:

$$C_2H_4Cl_2 + 4Ni \rightarrow 2[Ni–C] + 2[Ni–Cl] + 2H_2$$

$$[Ni–C] \rightarrow Ni + C\ (CNFs)$$

$$2[Ni–Cl] + H_2 \rightarrow 2Ni + 2HCl$$

In this case, the decomposition of DCE predominantly occurs through the formation of carbon nanofibers.

It is well known that catalytic performance of Ni metal can be substantially influenced by the introduction of various modifying elements or promotors. As it was recently reported, the addition of Cr [17] and Pd [18] into composition of Ni-M precursors allows one to enhance the productivity, while alloying Ni with Co or Cu did not show any significant advantage [17]. In the case of Ni-Cr system it was assumed that the presence of small amount of Cr (0.5 at.%) could play a decisive role in stabilization of the catalytic performance of Ni in the CCVD process [17].

As it is well known from voluminous literature, the addition of Mo metal is one of the popular ways to boost the catalytic activity of nickel in the CCVD synthesis of CNM [18, 19, 20, 21, 22] as well as in other industrially important catalytic reactions such as steam reforming of hydrocarbons [23, 24, 25]. Most of the research works are though dedicated to an improved synthesis of single- and multi-walled carbon nanotubes (CNTs), which requires high temperatures (800 °C and above) [18, 19, 20, 21]. Molybdenum was established to serve as a synergy component, which allows one to increase greatly the performance of the supported Ni-catalysts. Moreover, the addition of Mo was also found to have beneficial effect on the structural properties and quality of the produced CNT [19] and CNF [22] materials.

Thus, the investigation of impact of the Mo addition on the catalytic performance of Ni based self-organized catalysts used in CCVD of chlorinated HC is considered to have a fundamental character. Study on regularities of formation and functioning of the catalysts resulted from metal dusting of micro-disperse $Ni_{1-x}Mo_x$ alloys under the reaction conditions was the main objective of the present work. For this purpose, we have synthesized a series of the single-phase solid $Ni_{1-x}Mo_x$ solutions containing up to 8.3 wt.% Mo and studied the kinetic features of their interaction with $C_2H_4Cl_2$ (DCE) vapors in a carbon erosion regime. The effect of Mo content on the structural characteristics of the obtained carbon nanomaterial was also studied.

2. Experimental

2.1. Preparation of $Ni_{1-x}Mo_x$ solid solution

Synthesis of $Ni_{1-x}Mo_x$ solid solutions was carried out by the coprecipitation procedure followed by subsequent heating of resulted sediment in the reducing environment (H_2). Calculated amounts of precursor salts, $[Ni(NH_3)_6]Cl_2$ (synthesized by standard technique [26]) and $(NH_4)_6Mo_7O_{24}$ (Purissimum speciale) were dissolved in 30 mL of 10% ammonia solution. Mixed solution of metal salts was added to an excess of acetone (Purissimum speciale) that was previously cooled down to T ~ 0 °C. The resulted sediment of light violet color was filtered out, washed abundantly with acetone and dried at a room temperature for 12 h. Dried samples were afterwards reduced in a hydrogen flow (130 cm^3/min) at 800 °C for 1 h. Reduced Ni-Mo alloy samples were cooled down to a room temperature in a helium flow.

Content of Mo introduced into composition of the alloy was varied from 0.6 to 16 wt.%. The reference samples of unmodified nickel (100%-Ni) and pure molybdenum (100%-Mo) were also synthesized via the same procedures.

2.2. Catalytic decomposition of DCE

1,2-dichloroethane (DCE) was used in the catalytic CVD experiments as a model chlorinated hydrocarbon. The catalytic decomposition of DCE vapors over the studied samples was carried out in a specially designed flow quartz reactor equipped with McBain balances [26]. It allowed us to measure the weight of the sample in a real-time regime. Since the CCVD process was accompanied by rapid disintegration of pristine alloy along with intensive growth of carbon nanomaterial, the weight gain was used as an illustration of the process kinetics. The sample of Ni-Mo alloy (2.00 ± 0.02 mg) was loaded into a quartz basket connected to calibrated quartz spring by means of a long quartz wire. Prior to the CCVD experiment, each specimen was subjected to 30 min reduction in a hydrogen flow at 500 °C. After pretreatment the sample was brought to a contact with the reaction mixture ($DCE/H_2/Ar$ = 7.5/37.5/55, vol.%). Reaction temperature was varied within a range of 550–700 °C. The duration of the catalytic experiment was 2 h. At the end of the experiment the reactor was cooled down in an argon flow to a room temperature. The resulting sample of CNM was weighted using a Sartorius analytical balance, and the carbon yield was calculated with regard to the weight of initial specimen.

2.3. Characterization and measurements

2.3.1. Chemical analysis

The chemical composition of the synthesized Ni-Mo samples was determined by atomic absorption spectroscopy (AAS) on a Solaar IC-3000 spectrometer. Prior to measurement procedure, the metallic samples were dissolved in nitric acid.

2.3.2. X-ray diffraction analysis (XRD)

The powder XRD analysis of Ni-Mo samples was performed at a room temperature on a Shimadzu XRD-7000 diffractometer (CuKα radiation, Ni filter on the reflected beam). The patterns were recorded in the step mode within the angular range 2θ = 7–107°, step 0.05° (survey diffraction pattern) and 2θ = 140–147°, step 0.02° (for precise determination of unit cell parameter). Data from the PDF database were used as a reference [27]. The lattice parameters were calculated from (331) reflex diffraction data (2θ ≈ 144°) using the PowderCell 2.4 software. The volume-averaged crystallite sizes were determined from the integral broadening of the (111), (200), (220) peaks using the Scherrer equation [28], after separation of contribution from instrumental broadening. Deconvolution and fitting of the X-ray diffraction lines based on the Pearson (PVII) function was performed using the WinFit 1.2.1 software [29].

2.3.3. Scanning and transmission electron microscopy (SEM, TEM, EDX)

The morphology of both the synthesized micro-disperse Ni-Mo alloys and the produced CNM samples was explored by scanning electron microscopy (SEM) on a JEOL JSM6460 electron microscope with a

resolution of 4 nm.

Transmission electron microscopy (TEM) technique was used to examine the structural features of the obtained carbon product. TEM studies were performed on a JEM-1400 (JEOL, Japan) instrument at an accelerating voltage of 80 kV. Prior to being deposited onto TEM grid, CNM samples were carefully mixed with deionized water to obtain the CNM/H_2O suspensions. Such approach allowed us to minimize the damage that is commonly caused to rather brittle structure of carbon filaments during the regular sonication procedure.

The local chemical composition of catalytic particles was studied by means of scanning transmission electron microscopy (STEM) combined with energy dispersive spectrometer (EDX). STEM micrographs were obtained on HT-7700 microscope, Hitachi (Japan) which was equipped with an EDX spectrometer XFlash 6T/60, Bruker (Germany).

2.3.4. Raman spectroscopy

Structure of the obtained carbon nanomaterial was studied by Raman spectroscopy. Raman spectra of samples was collected on a Horiba Jobin Yvon HR800 laser Raman spectrometer equipped with a 1024 pixel CCD detector and 1800 g/mm grating using a 532-nm line 15 mW Nd:YAG laser. The Raman spectrometer was coupled with an Olympus BX41 microscope with a SLMPlan N 50× objective. The spectra were obtained in the back-scattering geometry using an input microscope with a spot diameter about ~2 μm.

2.3.5. Textural characterization

The low-temperature N_2 adsorption (BET method) was used to define the textural parameters of the produced CNM samples (specific surface area, SSA, m^2/g; pore volume, V(pore), cm^3/g; micropore volume, V(micro), cm^3/g; average pore diameter, d(pore), Å). The adsorption isotherms were measured at 77 K on ASAP-2400 (Micromeritics, USA).

3. Results and discussion

3.1. Characterization of Ni-Mo system

The phase composition of synthesized metallic Ni-Mo samples was explored by the XRD technique. The survey XRD profiles for the samples with different content of Mo are presented in Fig. 1. The reflexes detected within the 2θ region of 40–100° are typical for the face-centered cubic lattice (*fcc*) of nickel. The increase in Mo concentration (0.6–8.3 wt.%) is obviously seen to cause a characteristic shift in position of the reflexes towards the low-angle region, if compare to a reference sample (100%-Ni).

The XRD patterns recorded in the far angle region (2θ = 140–147°) are shown in Fig. 2. One can clearly see that increase in Mo content leads to a significant change in both the shape and position of the peaks corresponding to (331) reflex.

Thus, the absence of odd peaks on the XRD pattern along with the certain low-angle shift of reflexes allows one to suggest the formation of single-phase $Ni_{1-x}Mo_x$ alloys (random solid solution based on *fcc* crystal lattice of nickel) in the case when Mo content does not exceed the value of 8.3 wt.%. The prepared series of single-phase Ni-Mo samples was studied in further catalytic tests.

At the same time, the sample with the highest Mo concentration exhibited quite different phase composition (Fig. 1, top curve). Rise of Mo concentration up to 16 wt.% resulted in primary formation of the intermetallic Ni_4Mo phase. The observed phenomenon is in good agreement with the Mo-Ni binary phase diagram available from database [30]. Thus, this sample wasn't tested as a catalyst precursor in the decomposition of DCE.

Crystallographic data for Ni-Mo samples examined by XRD are summarized in Table 1. It is seen that an increase of Mo content in the alloy results in the corresponding increase of its lattice parameter (a) from 3.524(1) to 3.542(3) Å.

The calculated average crystallite size (coherent scattering region, CSR) for the Ni-Mo alloys was found to lie within the region of 12–44 nm, indicating the distinct tendency to decrease with the rise of Mo concentration. As follows from Fig. 2, the width of the diffraction peaks increases with increasing the Mo content, which is due to both the smaller crystallite sizes and minor deviations from the nominal composition in different crystallites. Such behavior might be explained by the influence of low diffusion activity of molybdenum which is known to be highly refractory metal (T_{melt} = 2623 °C). In this connection, the increase in Mo concentration is thought to slow down the rate of the solid solution formation and the growth of crystallites, thus leading to a smaller size of those.

The morphology and structure of the synthesized $Ni_{1-x}Mo_x$ alloys was studied by SEM technique. From the SEM micrographs presented in Fig. 3 for $Ni_{1-x}Mo_x$ alloy containing 8.3 wt.% Mo (as an example) one can see the sponge-like porous structure of alloy which is composed of interconnected ligaments with an average diameter of 1–3 μm. Observed images permit one to confirm that the diffusion rate of Ni and Mo atoms remains rather low even at sufficiently high temperature of reduction (800 °C), which prevents the adjacent alloy grains from agglomeration.

3.2. Catalytic studies of DCE decomposition

The synthesized samples of Ni-Mo alloys were tested in the process of

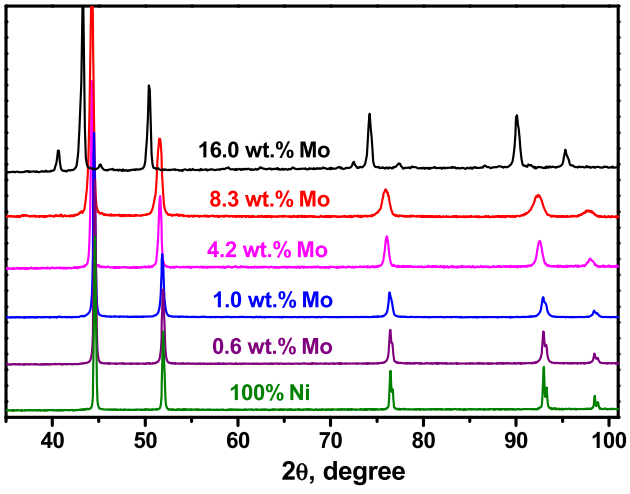

Fig. 1. Survey X-ray diffraction profiles for the series of Ni-Mo samples.

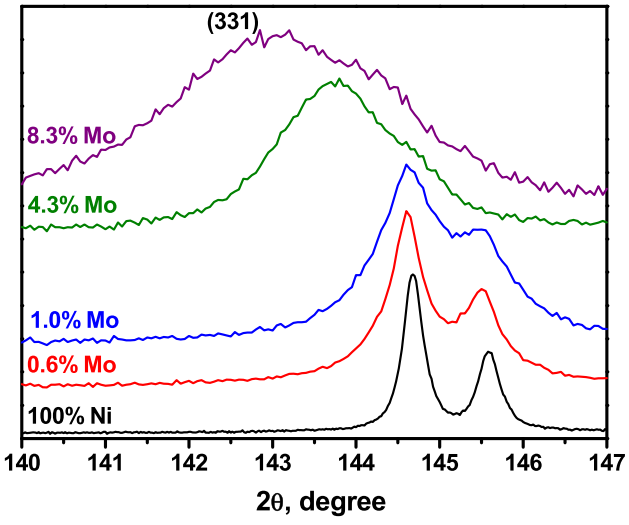

Fig. 2. XRD patterns of Ni-Mo alloys: reflex (331) in far angles.

Table 1
Crystallographic data for the synthesized Ni-Mo alloys.

#	Content of Mo in alloy, wt.% (*)	*a*, Å	Average crystallite size, nm
1	0	3.524(1)	90
2	0.6	3.524(1)	44
3	1.0	3.524(1)	32
4	4.2	3.534(2)	27
5	8.3	3.542(3)	12

(*) – in accordance with AAS data.

catalytic CVD of $C_2H_4Cl_2$ vapors (7.5 vol.) in a mixture with H_2 (37.5 vol.%) and argon (balance). Presence of excess hydrogen in combination with chlorinated HC facilitates the process of metal dusting that was earlier demonstrated for the bulk Ni-based alloys [11]. Moreover, addition of odd H_2 into reaction environment is known to exert positive impact on the catalytic performance, since it keeps the catalyst out from fast deactivation [10]. The reaction temperature was fixed to be 600 °C in order to make it possible to compare the catalytic behavior of Ni-Mo system with others Ni-M alloys tested before. Experiments were carried out in a flow regime using gravimetric setup (McBain balances), which allowed one to conduct the *in situ* kinetic measurements of the carbon deposition process. The obtained kinetic curves are presented in Fig. 4.

As follows from Fig. 4, the kinetics of carbon accumulation process is characterized with presence of distinct initial stage (i.e. induction period, IP), at which the observed weight gain does not exceed 100%. Appearance of IP is related to the first stage of the metal dusting process, when the carbon transfer to the alloy's surface, its diffusion into the bulk and subsequent nucleation of the graphite phase commonly take place [16, 31, 32]. It can be also seen that the content of Mo in the Ni-Mo alloy exerts significant influence upon the duration of observed IP (Fig. 4).

The effect of Mo content on the duration of IP is separately illustrated by Fig. 5 (left *y*-axis). On can clearly see that the introduction of Mo (even in small amount of 0.6 wt.%) leads to a dramatic drop of the induction period duration: from 20 min for 100%-Ni to 6 min for 8.3 wt.% Mo (Fig. 5).

It should be though emphasized that the most impressive finding of catalytic study is represented by the great positive impact of the Mo addition upon the catalytic performance of nickel. This fact is highlighted by the dependence of carbon yield (in grams of CNM per 1 g of a loaded metal, g/g_M) versus concentration of molybdenum shown in Fig. 5. One can obviously see that the rise of Mo concentration results in steady growth of catalyst's productivity that reaches the highest value of 45 g/g_M for the sample containing 8.3 wt.% of Mo which is more than 2 times higher than that for the reference 100%-Ni sample (Fig. 5, Table 2). The sample containing 16 wt.% of Mo was not tested since it was shown to be represented by different phase (Ni_4Mo, Fig. 1), thus leaving the question about the optimal Mo content still open. It is also worth noting that another reference sample, 100%-Mo, was found to be absolutely inactive under the same reaction conditions.

The highest yield of the CNM product obtained on Ni-Mo alloys outperforms the productivity of all other binary Ni-M systems (M = Fe, Co, Cu, Cr, Pd) that had been synthesized by similar preparative procedure and tested in the same reaction conditions. With aim to provide clear comparison, the information related to the best-performing samples selected from each Ni-M series studied before are collected in Table 2. It is apparent that the synthesized Ni-Mo alloy demonstrates the shortest duration of IP along with superior yield of carbon nanomaterial measured for 2 h of the CCVD process (Table 2).

It can be thus concluded that the alloying Ni with Mo (at

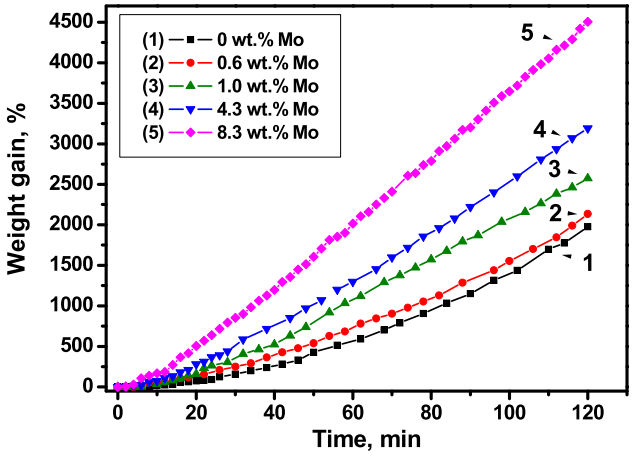

Fig. 4. Effect of Mo content on the kinetics of carbon deposition over $Ni_{1-x}Mo_x$ alloys. Reaction conditions: DCE/H_2/Ar, T = 600 °C.

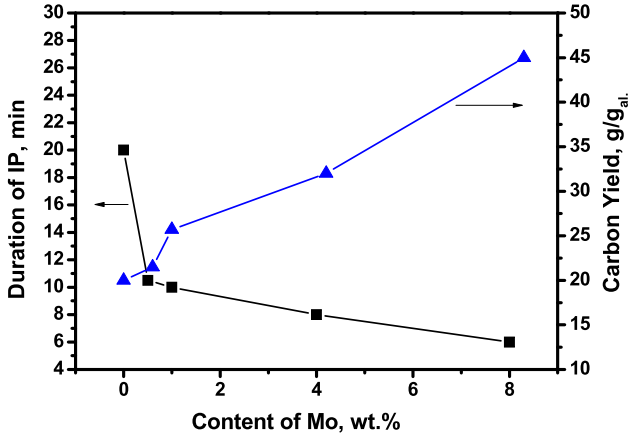

Fig. 5. Impact of Mo content (wt.%) in Ni-Mo alloy upon duration of induction period (IP) and carbon yield (in $g/g_{al.}$, grams of CNM per 1 g of loaded alloy) measured after 2 h. Reaction conditions: DCE/H_2/Ar, T = 600 °C.

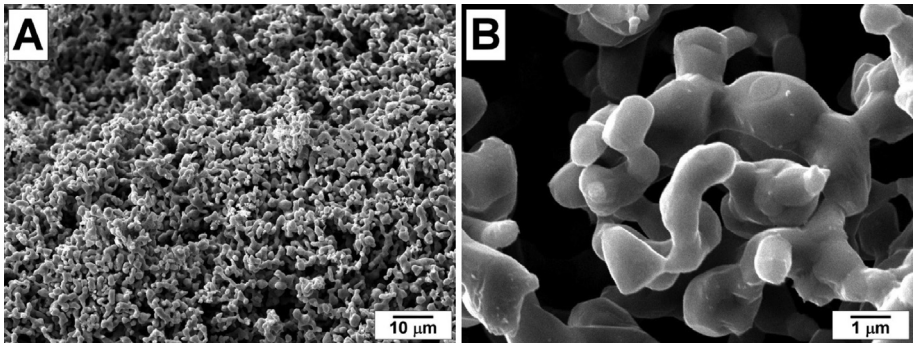

Fig. 3. SEM images of $Ni_{1-x}Mo_x$ alloy (8.3 wt.% Mo) sample after treatment in hydrogen at 800 °C. The magnification is x1,000 (A) and x10,000 (B).

Table 2
Effect of alloying metal (M) upon the catalytic performance of micro-dispersed Ni-M alloys. Reaction conditions: DCE/H_2/Ar, T = 600 °C, duration – 2 h. Recently published data are given for comparison.

No.	Metal M	Composition (*), wt. %	Duration of IP, min	Carbon Yield, g/g_M	Ref.
1	Ni reference	Ni-100	20	20	[17, 33]
2	Cr	Ni-95 Cr-5	17	24	[34]
3	Cu	Ni-99 Cu-1	20	27	[33]
4	Co	Ni-99 Co-1	22	26.5	[33]
5	Fe	Ni-90 Fe-10	40	3.5	[17]
6	Pd	Ni-95 Pd-5	22	22.5	[35]
7	Mo	Ni-92 Mo-8	6	45	present work

(*) – The best active sample from each Ni-M series is presented.

concentration of latter less than 10 wt.%) provides the emergence of a strong boosting effect on the catalytic performance of nickel. The observed behavior is in agreement with literature data concerning the synergistic impact of Mo on activity of iron subgroup metals (Fe, Co, Ni) in the CCVD synthesis of carbon nanotubes and nanofibers [18, 19, 20, 21, 22, 36, 37].

The effect of reaction temperature upon the catalytic performance was studied for the case of the most active Ni-Mo alloy (8.3 % Mo). The reaction temperature was varied in the range of 550–700 °C. The obtained temperature dependence of carbon yield after 2 h of experiment is represented by Fig. 6.

From the results obtained one may suggest that the optimal temperature regime for the DCE decomposition over Ni-Mo system should be ranged somewhere between 600 and 650 °C (Fig. 6). At the reaction temperature of 550 °C and below the process of carbon erosion of metal alloy appears to occur much slower because of hindering function of surface Cl species. Further decrease of temperature may result in almost complete suppression due to full chlorination of nickel [38]. On the other hand, elevation of reaction temperature to 700 °C and above again leads to deceleration of metal dusting process. Such tendency is caused by the enhanced deposition rate of the amorphous carbon, which encapsulates the surface of metallic alloy, thus preventing it from further interaction with the reaction mixture. This observation agrees well with earlier researches where the existence of optimal window for the rate of metal dusting was established [39].

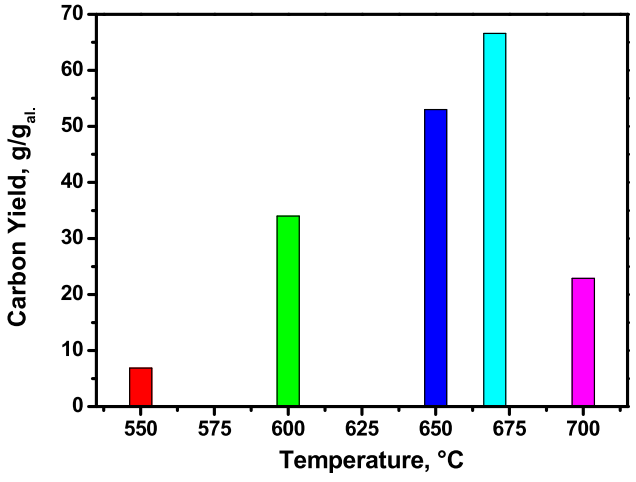

Fig. 6. Impact of reaction temperature upon carbon yield after 2 h of $C_2H_4Cl_2$ decomposition over Ni-Mo alloy (8.3 wt.% Mo). Reaction conditions: DCE/H_2/Ar.

Additionally, the kinetic curves of CNM accumulation during the DCE decomposition in a temperature range of 600–670 °C were used for the evaluation of the apparent activation energy (E_a) of the reaction. Table 3 summarized initial data for the calculation of E_a. According to these data, the activation energy was estimated to be 68 ± 4 kJ/mol. This allows us to assume that the decomposition of DCE (the supply of carbon atoms) is a rate-limiting step of the process of CNM deposition, whereas the diffusion of carbon atoms in the alloy is a rapid step, which does not influence the rate of the overall process.

3.3. Morphology and structure of carbon product

As seen from Fig. 7, carbon nanomaterial produced by decomposition of DCE over Ni-Mo alloys is mainly represented by carbon fibers of submicron diameter. The similar structure of carbon fibers is observed for the reference 100%-Ni sample shown for comparison (Fig. 7 A, B).

Dark-field SEM image of CNM sample presented in Fig. 7C permits one to see the obvious presence of disperse metallic particles appeared as bright spots of white color. Observed crystals are known to play a role of the active centers responsible for the catalytic conversion of DCE as well as for the deposition of filamentous carbon product. Active particles catalyzing the CNM growth are derived from the spontaneous disintegration of pristine Ni-Mo alloys driven by the intensive carbon erosion process (i.e. metal dusting) under action of aggressive reaction environment. It can be thus claimed that the interaction of micro-disperse Ni-Mo alloy with $C_2H_4Cl_2$ vapors is accompanied by its complete wastage to give the rise of submicron catalytically active particles producing the nanostructured carbon material.

A set of SEM images collected in Fig. 7 is focused on elucidating the effect of Mo content in Ni-Mo alloy on morphology of the produced CNM. It may be noticed that samples with low Mo content (0.6 and 1.0 wt.%, Fig. 7 C–F) are composed of bundles of rather long and straight carbon filaments. At the same time, CNM produced over Ni-Mo samples containing 4.2 and 8.3 wt.% Mo is represented by chaotically intermixed fibers that are noticeably shorter in length and thinner in diameter (Fig. 7 G–J). The observed gradual deprivation of the filamentous character of CNM with the increase of Mo concentration might be explained by significant difference in a rate of carbon deposition, which has been discussed above (Fig. 5).

As it also can be observed from the presented SEM images (Fig. 7), the obtained carbon filaments are characterized by well-expressed segmental structure. The segmented structure of carbon fibers is formed by more or less regular alteration of graphene areas with different density of packing. This fact can be the most obviously illustrated by the selected TEM micrographs shown in Fig. 8. TEM image presented in Fig. 8B demonstrates the fragment of fiber with segmented structure which is built by a set of dense graphite “flakes” (dark strips) interchanged with loose areas filled with less dense matter. Careful examination of the fiber's end face allows one to discern the fine nanoscale composition that could be named as “mosaic structure”, which is represented by an ensemble of the separate graphite units of about 15–20 nm in size (Fig. 8B).

The growth of segmented carbon fibers is apparently catalyzed by the active metallic particles. The example of such catalytic center of the CNM

Table 3
Initial kinetic data on the CNM deposition over Ni-Mo alloy (8.3 wt.% Mo) during the DCE decomposition.

Temperature		w^*, mg/min	ln$w$	1000/T, K^{-1}
°C	K			
600	873	0.297	-1.215	1.145
630	903	0.443	-0.813	1.107
650	923	0.483	-0.727	1.083
670	943	0.612	-0.491	1.060

* Calculated from the kinetic curves for a reaction time range of 40–100 min.

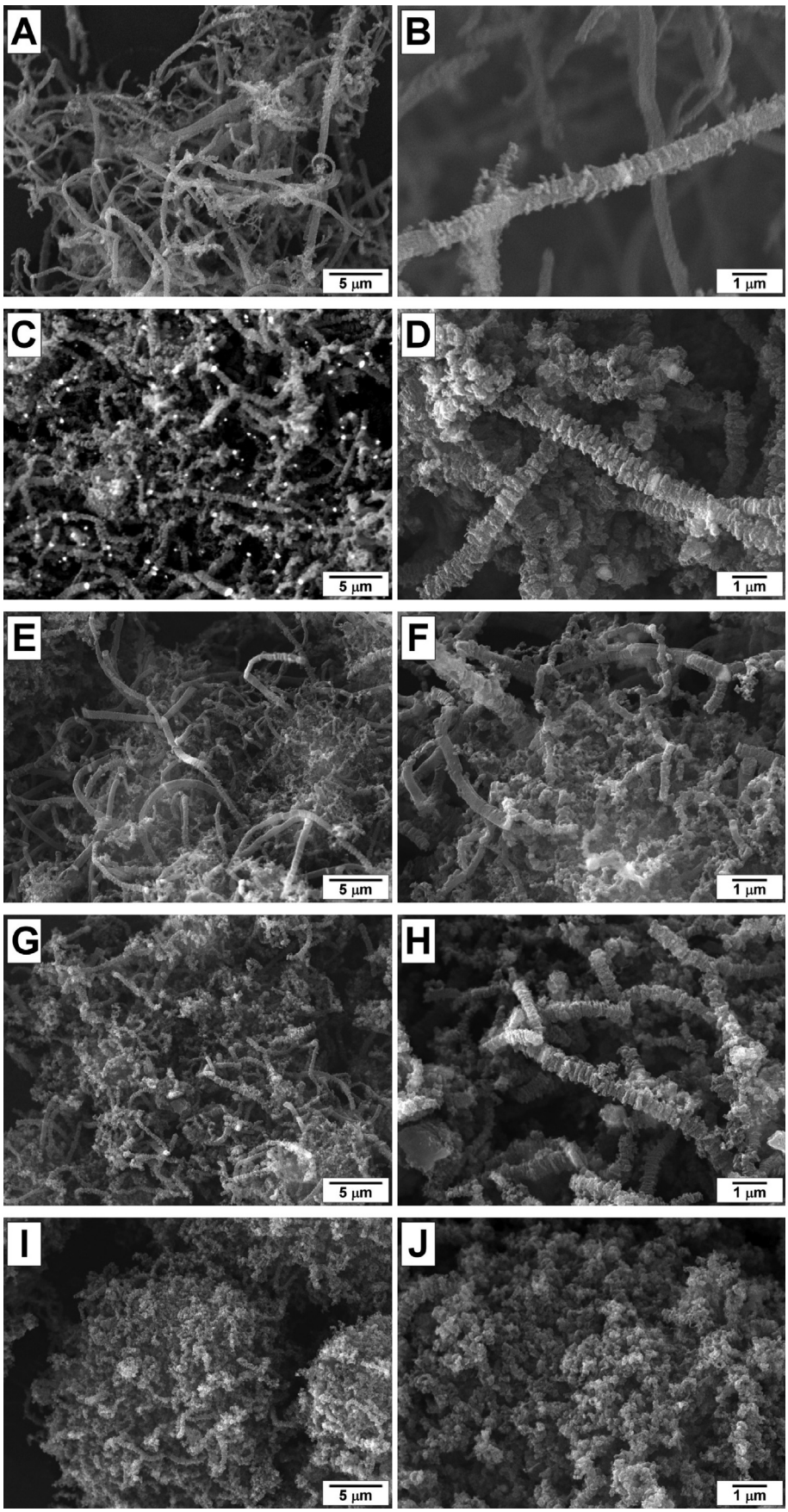

Fig. 7. SEM images of carbon material produced by decomposition of DCE over Ni-Mo alloys: A, B – 0 wt.% Mo (100% Ni); C, D – 0.6 wt.% Mo; E, F – 1.0 wt.% Mo; G, H – 4.2 wt.% Mo; I, J – 8.3 wt.% Mo. Reaction conditions: DCE/H_2/Ar, T = 600 °C, duration – 2 h.

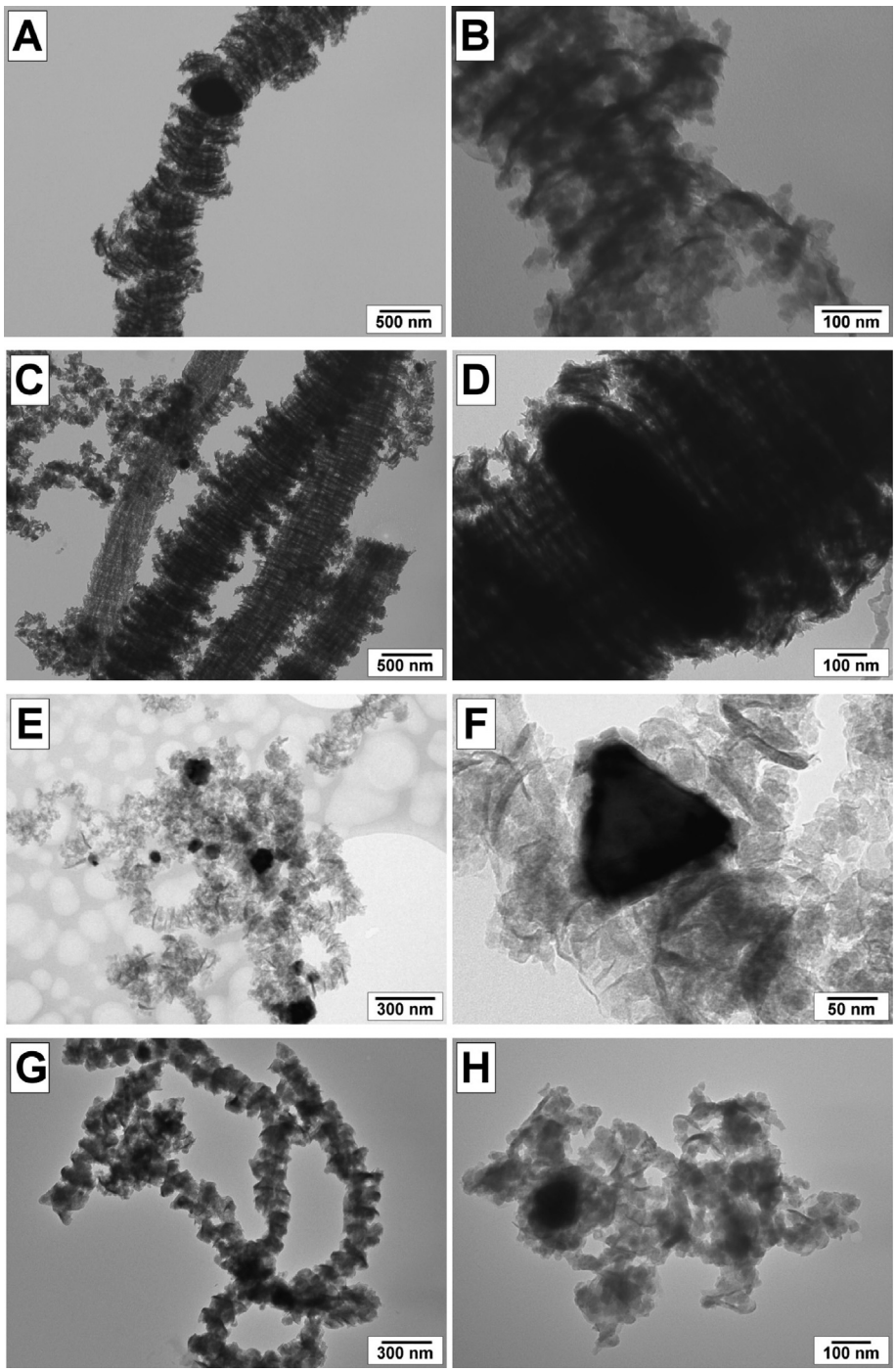

Fig. 8. TEM images of carbon filaments obtained by decomposition of DCE over Ni-Mo alloys: A, B – 0.6 wt.% Mo; C, D – 1.0 wt.% Mo; E, F – 4.2 wt.% Mo, G, H – 8.3 wt.% Mo. Reaction conditions: DCE/H_2/Ar, T = 600 °C, duration – 2 h.

growth can be seen from Fig. 8D. This particle has comparatively big size (close to 1 micron) and rather symmetric shape. This feature seems to determine the preferential type of CNF formation – double-sided growth in two antiparallel directions. It is worth to note that observed carbon fiber resembles the 2D-framework (grid), which is composed by the perpendicular crossing of the graphene strips (Fig. 8D). The formation mechanism of so-called "2D-segmental" fibers still remains unclear.

Interestingly that an increase in Mo content in Ni-Mo alloy results in distinct transformation of the segmental structure as illustrated by Fig. 8E–H. While the large particles preserves the tendency towards formation of filaments (Fig. 8G), the smaller ones (less than 200 nm in diameter) seem to lose the ability to grow well-structured carbon fibers (Fig. 8H). Disintegration of Ni-Mo (8.3 wt.% Mo) sample is appeared to occur with formation of the smaller crystallites that in general correlates with tendency observed by XRD for the pristine Ni-Mo materials (Table 1).

Fig. 9A shows the STEM micrograph of the active metallic particle that was formed in course of DCE decomposition over Ni-Mo (4.2 wt.%) sample at 600 °C. This particle is seen to be attached to three carbon fibers of about 250–400 nm in diameter. The mapping data of the principle elements present in designated cartography zone are shown in Fig. 9 B–D. The obtained results confirmed that the active particle is mainly composed of two metals – Ni and Mo. Nickel appears to be strictly localized within the boundaries of the metallic crystal (Fig. 9 B), while

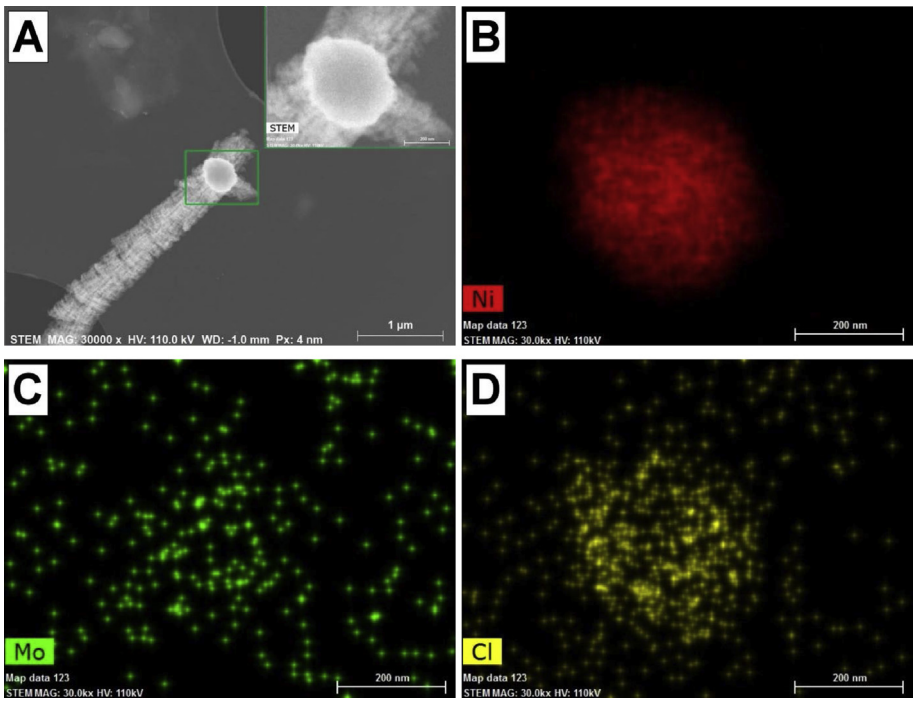

Fig. 9. STEM image of the cartography zone (A) and elemental mappings of Ni (B), Mo (C) and Cl (D) of the Ni-Mo alloy (4.2 wt.% Mo) sample. Reaction conditions: DCE/H_2/Ar, T = 600 °C, duration - 2 h.

the molybdenum did not exhibit any preferential localization (Fig. 9 C).

It has to be noted that the elemental mapping also revealed the presence of a considerable amount of Cl that tends to be basically concentrated over the surface of the metallic particle (Fig. 9 D). Strongly chemisorbed chlorine species are believed to be responsible for the emergence of the certain perturbations in carbon transfer and nucleation of the graphite phase [35, 40, 41]. Some part of residual chlorine was reported to be always present within the composition of CNM produced by the catalytic CVD of various chlorinated hydrocarbons [7, 8, 12].

It should be emphasized that the presence of halogen (chlorine) in the reaction system is believed to have a decisive impact on the structural features of CNM produced from halogenated (chlorinated) hydrocarbons. So, the formation of carbon filaments with segmental (or mosaic) structure is assumed to be determined by the ever-interrupted diffusion flux of carbon atoms through the active metal particle. Pulse-to-pulse character of carbon deposition occurs due to the cyclic "chlorination/dechlorination" process upon the metallic surface, at which the decomposition of $C_2H_4Cl_2$ molecules takes place [35].

Fig. 10 demonstrates the Raman spectra of carbon materials obtained by decomposition of $C_2H_4Cl_2$ vapors over Ni-Mo alloys (C_{Mo} = 0–8.3 wt.%) at the same temperature (600 °C).

All spectra are seen to exhibit the G peak at ~1580 cm^{-1} corresponding to allowed E_{2g} vibration mode of the graphite hexagons [42] and rather intensive disorder induced D line at about 1340 cm^{-1} (activated A_{1g} mode) due to the finite crystal size [43, 44]. The second-order lines (2D at ~2680 cm^{-1}) were found to be low-intensive and independent from Mo content in alloy. The most noticeable change in Raman spectra were observed for CNM produced on Ni-Mo (1.0 wt.% Mo) sample which showed both the increase of I_D/I_G ratio from 1.71 to 1.99 and narrowing of the half-width of D line from 80 cm^{-1} to 70 cm^{-1}, if compare to the reference 100%-Ni sample (Fig. 10, inset). Based on known correlation $I_D/I_G \sim C_l L_a^2$ [44] and the excitation wavelength λ = 532 nm, one may calculate that the observed change of I_D/I_G ratio corresponds to an increase of graphene cluster size from L_a~15.5 Å to L_a~17 Å. Further rise of Mo concentration (4.2, 8.3 wt.%) results in a certain decrease of the cluster size that might be accounted for considerable increase of the CNM growth rate.

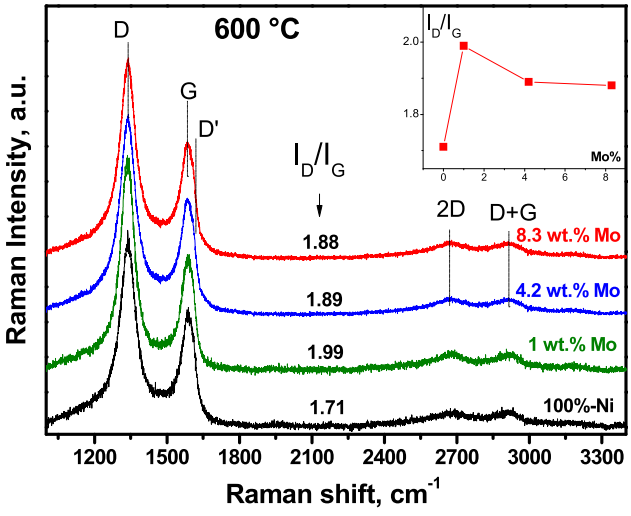

Fig. 10. Raman spectra of CNM samples produced over Ni-Mo alloys with different Mo content (0–8.3 wt.%). Reaction conditions: DCE/H_2/Ar, T = 600 °C, duration - 2 h. Dependence of I_D/I_G upon Mo content is shown on inset.

Textural properties (measured by BET method) of the CNM samples produced over Ni-Mo alloys with different molybdenum concentration are given in Table 4. All obtained carbon materials are seen to be characterized with comparatively high specific surface area (~300 m^2/g and above) and rather developed porosity (0.5–0.7 cm^3/g). Corresponding adsorption isotherms are shown in Fig. 11. From the results presented in Table 4 one can see that the highest SSA value (370 m^2/g) belongs to the Ni-Mo (4.2 wt.% Mo) sample while the minimal one (290 m^2/g) was observed in case of Ni-Mo alloy containing 8.3 wt.% of Mo. It corresponds to a slight difference in contribution of micropores, which is connected with structural changes shown in Fig. 8. Determined values are in good agreement with recently published data concerning the textural features of the segmental carbon filaments obtained by decomposition of DCE on

Table 4
Influence of Mo content in Ni-Mo alloy upon the textural properties of the produced CNM. Reaction conditions: DCE/H_2/Ar, T = 600 °C, duration – 2 h.

No.	Content of Mo (vol.%)	Y_C, g/g_{Ni}	SSA, m^2/g	V(pore), cm^3/g	V(micro), cm^3/g	Average d(pore), 4V/A by BET, Å
1	0.6	18.6	324	0.50	0.076	66.89
2	1.0	25.8	320	0.70	0.065	94.83
3	4.2	32.6	370	0.66	0.078	78.89
4	8.3	47.2	290	0.65	0.063	96.84

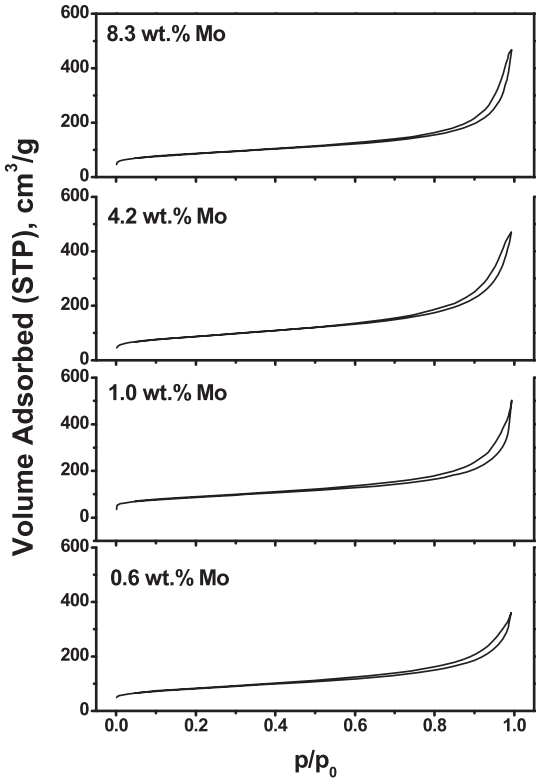

Fig. 11. Low-temperature nitrogen adsorption isotherms for CNM samples produced over Ni-Mo alloys with different Mo content (0.6–8.3 wt.%). Reaction conditions: DCE/H_2/Ar, T = 600 °C, duration - 2 h.

various micro-disperse Ni-M alloys (M = Co, Cu, Cr, Pd) [17, 34, 35, 36].

4. Conclusion

Self-organizing Ni-based catalysts resulted from the controllable metal dusting of Ni-M precursor alloys are known to be effective in processing of chlorinated hydrocarbons and associated waste products into filamentous carbon nanomaterials. The present research was aimed to study the effect of Mo addition upon the catalytic activity of Ni in CCVD process of 1,2-dichloroethane with formation of the CNM product. Based on results obtained it is possible to make the following conclusions:

1. A method of simultaneous precipitation with subsequent sintering in reducing atmosphere was successfully implemented for the synthesis of the micro-disperse $Ni_{1-x}Mo_x$ alloys. A detailed XRD study revealed the formation of single-phase solid solution with *fcc* lattice for the Mo concentration ranged within 0.6–8.3 wt.%. It was found that the average crystallite size tends to decrease with the rise of molybdenum content which is explained by the low diffusion rate of Mo. Synthesized Ni-Mo alloys were shown to possess rather developed sponge-like structure composed by the interconnected secondary particles of about 1–3 μm in diameter.
2. Kinetics of DCE decomposition over the prepared Ni-Mo alloys was studied in standard reaction conditions in order to make it possible to compare the results with earlier published data. Interaction of Ni-Mo samples with DCE vapors results in quick disintegration of micro-disperse alloys with formation of submicron active particles catalyzing the growth of carbon filaments. The great positive impact of Mo on catalytic behavior of Ni was established. The carbon productivity (600 °C, 2 h) of the most active Ni-Mo (8.3 wt.%) sample was as high as 45 g/g_M which can be referred as outstanding performance among all the Ni-M alloys tested before. The range of 600–650 °C was found to be the optimal temperature window for an implementation of the reaction over Ni-Mo system.
3. Microscopic studies have revealed that the obtained CNM product is mostly represented by carbon filaments. They were shown to be characterized with the segmental structure which is formed by the regular alteration of graphene areas with different packing density. Emergence of the segmental structure of CNM was suggested to be driven by the presence of the chemisorbed Cl species on metallic surface which brings the certain perturbations in carbon diffusion and graphite nucleation. An increase in Mo concentration in pristine Ni-Mo alloys leads to formation of shorter carbon fibers with smaller diameter that might be explained by the significant difference in the rate of the carbon deposition.

The developed self-organizing Ni-Mo system can be effectively applied in the catalytic processing of chlorinated hydrocarbons, thus allowing one to retrieve carbon from wastes in the form of segmented filaments. If necessary, the residual catalytic particles (1–2 wt.%) might be easily removed from the composition of the carbon product by means of a conventional etching in diluted HCl acid. The high specific area of the segmented CNF along with their unique secondary structure makes this type of carbon nanomaterials attractive for various directions of application, including electrochemistry [45, 46], adsorption [47], catalysis [48, 49] and some other areas.

Declarations

Author contribution statement

Yury Bauman, Yuliya Rudneva, Denis Korneev & Vladimir Stoyanovskii: Performed the experiments.

Ilya Mishakov & Aleksey Vedyagin: Conceived and designed the experiments; Wrote the paper.

Pavel Plyusnin & Yury Shubin: Analyzed and interpreted the data.

Roman Buyanov: Conceived and designed the experiments.

Funding statement

This work was supported by the Russian Foundation for Basic Research (Project 18-29-19053 mk) and the Ministry of Science and Higher Education of the Russian Federation (Project 03-03-2016-0014).

Competing interest statement

The authors declare no conflict of interest.

Additional information

No additional information is available for this paper.

Acknowledgements

The authors are grateful to Dr. Maxim S. Mel'gunov for his assistance in textural characterization.

References

[1] E. Hammel, X. Tang, M. Trampert, T. Schmitt, K. Mauthner, A. Eder, et al., Carbon nanofibers for composite applications, Carbon 42 (52–56) (2004) 1153–1158.

[2] J.H. Kang, D.H. Shin, K.N. Yun, F.A. Masud, C.J. Lee, M.J. Kim, Super growth of vertically-aligned carbon nanofibers and their field emission properties, Carbon 79 (2014) 149–155.

[3] A. Magrez, J.W. Seo, R. Smajda, M. Mionic, L. Forro, Catalytic CVD synthesis of carbon nanotubes: towards high yield and low temperature growth, Mater 3 (11) (2010) 4871–4891.

[4] J.H. Zhou, Z.J. Sui, P. Li, D. Chen, Y.C. Dai, W.K. Yuan, Structural characterization of carbon nanofibers formed from different carbon-containing gases, Carbon 44 (2006) 3255–3262.

[5] E.C. Vermisoglou, G. Pilatos, G.E. Romanos, G.N. Karanikolos, N. Boukos, K. Mertis, et al., Synthesis and characterisation of carbon nanotube modified anodised alumina membranes, Micropor. Mesopor. Mater. 110 (1) (2008) 25–36.

[6] T. Iwasaki, Y. Makino, M. Fukukawa, H. Nakamura, S. Watano, Low-temperature growth of nitrogen-doped carbon nanofibers by acetonitrile catalytic CVD using Ni-based catalysts, Appl. Nanosci. 6 (8) (2016) 1211–1218.

[7] A. Shaikjee, N.J. Coville, The effect of substituted alkynes on nickel catalyst morphology and carbon fiber growth, Carbon 50 (3) (2012) 1099–1108.

[8] A. Nieto-Marquez, J.L. Valverde, M.A. Keane, Catalytic growth of structured carbon from chloro-hydrocarbons, Appl. Catal. Gen. 332 (2) (2007) 237–246.

[9] I.V. Mishakov, V.V. Chesnokov, R.A. Buyanov, N.A. Pakhomov, Decomposition of chlorinated hydrocarbons on iron-group metals, Kinet. Catal. 42 (4) (2001) 543–548.

[10] Y.I. Bauman, I.V. Mishakov, D.V. Korneev, Y.V. Shubin, A.A. Vedyagin, R.A. Buyanov, Comparative study of 1,2-dichlorethane decomposition over Ni-based catalysts with formation of filamentous carbon, Catal. Today 301 (2018) 147–152.

[11] Bauman YuI, I.V. Mishakov, R.A. Buyanov, A.A. Vedyagin, A.M. Volodin, Kinet catal catalytic properties of massive Iron_Subgroup metals in dichloroethane decomposition into carbon, Products 42 (4) (2011) 547–554.

[12] Bauman YuI, I.V. Mishakov, A.A. Vedyagin, S.V. Dmitriev, M.S. Mel'gunov, R.A. Buyanov, Processing of organochlorine waste components on bulk metal catalysts, Catal. Ind. 4 (4) (2012) 261–266.

[13] R.A. Buyanov, I.V. Mishakov, A.A. Vedyagin, Preparation of carbon nanomaterials in the process of organochlorine waste utilization, Solid Fuel Chem. 48 (3) (2014) 203–207.

[14] Y.I. Bauman, I.V. Mishakov, A.A. Vedyagin, S. Ramakrishna, Synthesis of bimodal carbon structures via metal dusting of Ni-based alloys, Mater. Lett. 201 (2017) 70–73.

[15] I.V. Mishakov, Bauman YuI, D.V. Korneev, A.A. Vedyagin, Metal dusting as a route to produce active catalyst for processing chlorinated hydrocarbons into carbon nanomaterials, Top. Catal. 56 (11) (2013) 1026–1032.

[16] P. Szakalos, R. Pettersson, S. Hertzman, An active corrosion mechanism for metal dusting on 304L stainless steel, Corros. Sci. 44 (2002) 2253–2270.

[17] Y.I. Bauman, I.V. Mishakov, A.A. Vedyagin, A.V. Rudnev, P.E. Plyusnin, YuV. Shubin, et al., Promoting effect of Co, Cu, Cr and Fe on activity of Ni-based alloys in catalytic processing of chlorinated hydrocarbons, Top. Catal. 60 (1-2) (2017) 171–177.

[18] L.P. Zhou, K. Ohta, K. Kuroda, N. Lei, K. Matsuishi, L. Gao, et al., Catalytic functions of Mo/Ni/MgO in the synthesis of thin carbon nanotubes, J. Phys. Chem. B 109 (10) (2005) 4439–4447.

[19] E.V. Lobiak, E.V. Shlyakhova, L.G. Bulusheva, P.E. Plyusnin, YuV. Shubin, A.V. Okotrub, Ni–Mo and Co–Mo alloy nanoparticles for catalytic chemical vapor deposition synthesis of carbon nanotubes, J. Alloy. Comp. 621 (2015) 351–356.

[20] Y. Li, X.B. Zhang, X.Y. Tao, J.M. Xu, W.Z. Huang, J.H. Luo, et al., Mass production of high-quality multi-walled carbon nanotube bundles on a Ni/Mo/MgO catalys, Carbon 43 (2) (2005) 295–301.

[21] R. Song, Q. Ji, Synthesis of carbon nanotubes from polypropylene in the presence of Ni/Mo/MgO catalysts via combustion, Chem. Lett. 40 (10) (2011) 1110–1112.

[22] E. Jang, H.K. Park, J.H. Choi, C.S. Lee, Synthesis and characterization of carbon nanofibers grown on Ni and Mo catalysts by chemical vapor deposition, Bull. Korean Chem. Soc. 36 (5) (2015) 1452–1459.

[23] T. Borowiecki, W. Gac, A. Denis, Effects of small MoO3 additions on the properties of nickel catalysts for the steam reforming of hydrocarbons: III. Reduction of Ni-Mo/Al2O3 catalysts, Appl. Catal. Gen. 270 (1-2) (2004) 27–36.

[24] S.S. Maluf, E.M. Assaf, Ni catalysts with Mo promoter for methane steam reforming, Fuel 88 (9) (2009) 1547–1553.

[25] Z.O. Malaibari, A. Amin, E. Croiset, W. Epling, Performance characteristics of MoeNi/Al2O3 catalysts in LPG oxidative steam reforming for hydrogen production, Int. J. Hydrogen Energy 39 (19) (2014) 10061–10073.

[26] G. Brauer, Handbuch der präparativen anorganischen Chemie, third ed., Enke, Stuttgart, 1981.

[27] Powder Diffraction File, PDF-2/Release, International Centre for Diffraction Data, USA, 2009.

[28] B.D. Cullity, Elements of X-ray Diffraction, second ed., Addison-Wesley Publishing Company, Massachusetts, 1978.

[29] S. Krumm, An interactive windows program for profile fitting and size/strain analysis, Mater. Sci. Forum 228–231 (1996) 183–188.

[30] Mo-Ni Binary Phase Diagram 0-100 at.% Ni: Datasheet from PAULING FILE Multinaries Edition, SpringerMaterials, Springer-Verlag Berlin Heidelberg & Material Phases Data System (MPDS), Switzerland & National Institute for Materials Science (NIMS), Japan, 2016. https://materials.springer.com/isp/phase-diagram/docs/c_0907678.

[31] H. Ghorbani, A.M. Rashidi, S. Rastegari, S. Mirdamadi, M. Alaei, Mass production of multi-wall carbon nanotubes by metal dusting process with high yield, Mater. Res. Bull. 46 (5) (2011) 716–721.

[32] M. Szkodo, G. Gajowiec, Studies of the mechanism of metal dusting of 10CrMo9-10 steel after10 years of operation in the semi-regenerative catalytic reformer, Corros. Sci. 102 (2016) 279–290.

[33] A.V. Rudnev, A.S. Lysakova, P.E. Plyusnin, Bauman YuI, YuV. Shubin, I.V. Mishakov, et al., Ni–Cu and Ni–Co alloys: synthesis, structure, and catalytic activity for the decomposition of chlorinated hydrocarbons, Inorg. Mater. 50 (6) (2014) 566–571.

[34] Bauman YuI, A.S. Lysakova, A.V. Rudnev, I.V. Mishakov, YuV. Shubin, A.A. Vedyagin, et al., Synthesis of nanostructured carbon fibers from chlorohydrocarbons over bulk Ni–Cr alloys, Nanotechnol. Rus. 9 (7-8) (2014) 380–385.

[35] Bauman YuI, YuV. Shorstkaya, I.V. Mishakov, P.E. Plyusnin, YuV. Shubin, D.V. Korneev, et al., Conversion of 1,2-dichloroethane over Ni-Pd system into filamentous carbon material, Catal. Today 293–294 (2017) 23–32.

[36] S. Tang, Z. Zhong, Z. Xiong, L. Sun, L. Liu, J. Lin, et al., Controlled growth of single-walled carbon nanotubes by catalytic decomposition of CH_4 over Mo/Co/MgO catalysts, Chem. Phys. Lett. 350 (1-2) (2001) 19–26.

[37] M.A. Kazakova, V.L. Kuznetsov, S.N. Bokova-Sirosh, D.V. Krasnikov, G.V. Golubtsov, A.I. Romanenko, et al., Fe–Mo and Co–Mo catalysts with varying composition for multi-walled carbon nanotube growth, Phys. Status Solidi B 255 (1) (2018) 1700260.

[38] Bauman YuI, I.V. Mishakov, A.A. Vedyagin, A.N. Serkova, A.A. Gromov, Kinetic features of carbon erosion of bulk Ni-Cr alloy during catalytic decomposition of 1,2-dichloroethane, Kinet. Catal. 58 (4) (2017) 448–454.

[39] C.M. Chun, G. Bhargava, T.A. Ramanarayanan, Metal dusting corrosion of nickel-based alloys, J. Electrochem. Soc. 154 (5) (2007) 231–241.

[40] A. Chambers, R.T.K. Baker, Influence of chlorine on the decomposition of ethylene over iron and cobalt particles, J. Phys. Chem. B 101 (9) (1997) 1621–1630.

[41] H.J. Grabke, M. Spiegel, A. Zahs, Role of alloying elements and carbides in the chlorine-induced corrosion of steels and alloys, J. Mater. Res. 7 (1) (2004) 89–95.

[42] R.J. Nemanich, S.A. Solin, First-and second-order Raman scattering from finite-size crystals of graphite, Phys. Rev. B 20 (2) (1979) 392–401.

[43] F. Tuinstra, J.L. Koenig, The theory behind FTIR, J. Chem. Phys. 53 (1970) 1126–1130.

[44] A.C. Ferrari, J. Robertson, Interpretation of Raman spectra of disordered and amorphous carbon, Phys. Rev. B 61 (20) (2000) 14095–14107.

[45] Z. Wang, L. Qie, L. Yuan, W. Zhang, X. Hu, Y. Huang, Functionalized N-doped interconnected carbon nanofibers as an anode material for sodium-ion storage with excellent performance, Carbon 55 (2013) 328–334.

[46] B. Zhang, F. Kang, J.M. Tarascon, J.K. Kim, Recent advances in electrospun carbon nanofibers and their application in electrochemical energy storage, Prog. Mater. Sci. 76 (2016) 319–380.

[47] H.K. Bong, S.M. Pestov, V.R. Flid, A.R. Karaeva, B.V. Peshnev, The adsorption properties of the sorbents based on nanofibrous carbon, OJAppS 7 (12) (2017) 720–728.

[48] M. Soria-Sanchez, A. Maroto-Valiente, J. Alvarez-Rodrıguez, I. Rodrıguez-Ramos, A. Guerrero-Ruız, Efficient catalytic wet oxidation of phenol using iron acetylacetonate complexes anchored on carbon nanofibres, Carbon 47 (2009) 2095–2102.

[49] X. Li, Y. Tuo, P. Li, X. Duan, H. Jiang, X. Zhou, Effects of carbon support on microwave-assisted catalytic dehydrogenation of decalin, Carbon 76 (2014) 775–783.